

A hybrid fuel cell for water purification and simultaneously electricity generation

Yujun Zhou^{1,3}, Qinghua Ji (✉)², Chengzhi Hu¹, Huijuan Liu², Juhui Qu^{1,2}

¹ Key Laboratory of Drinking Water Science and Technology, Research Center for Eco-Environmental Sciences, Chinese Academy of Sciences, Beijing 100085, China

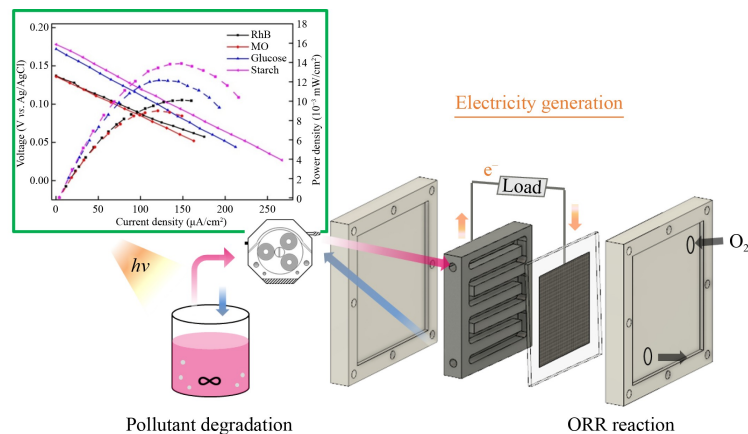
² Center for Water and Ecology, State Key Joint Laboratory of Environment Simulation and Pollution Control, School of Environment, Tsinghua University, Beijing 100084, China

³ Jiangsu Key Laboratory of Chemical Pollution Control and Resources Reuse, School of Environmental and Biological Engineering, Nanjing University of Science and Technology, Nanjing 210094, China

HIGHLIGHTS

- A novel hybrid fuel cell (F-HFC) was fabricated.
- Pollutant degradation and synchronous electricity generation occurred in F-HFC.
- BiOCl-NH₄PTA photocatalyst greatly improved electron transfer and charge separation.
- Pollutant could act as substrate directly in ambient conditions without pretreatment.
- The mechanism of the F-HFC was proposed and elucidated.

GRAPHIC ABSTRACT



ARTICLE INFO

Article history:

Received 20 December 2021

Revised 27 July 2022

Accepted 30 July 2022

Available online 31 August 2022

Keywords:

Flow-through field

Hybrid fuel cell

Polyoxometalates

Water purification

Electricity generation

ABSTRACT

The development of highly efficient energy conversion technologies to extract energy from wastewater is urgently needed, especially in facing of increasing energy and environment burdens. Here, we successfully fabricated a novel hybrid fuel cell with BiOCl-NH₄PTA as photocatalyst. The polyoxometalate (NH₄PTA) act as the acceptor of photoelectrons and could retard the recombination of photogenerated electrons and holes, which lead to superior photocatalytic degradation. By utilizing BiOCl-NH₄PTA as photocatalysts and Pt/C air-cathode, we successfully constructed an electron and mass transfer enhanced photocatalytic hybrid fuel cell with flow-through field (F-HFC). In this novel fuel cell, dyes and biomass could be directly degraded and stable power output could be obtained. About 87 % of dyes could be degraded in 30 min irradiation and nearly 100 % removed within 90 min. The current density could reach up to ~267.1 $\mu\text{A}/\text{cm}^2$, with maximum power density (P_{\max}) of ~16.2 $\mu\text{W}/\text{cm}^2$, 12.2 $\mu\text{W}/\text{cm}^2$, and 13.9 $\mu\text{W}/\text{cm}^2$ when using methyl orange (MO), glucose and starch as substrates, respectively. This hybrid fuel cell with BiOCl-NH₄PTA composite fulfills the purpose of decontamination of aqueous organic pollutants and synchronous electricity generation. Moreover, the novel design cell with separated photodegradation unit and the electricity generation unit could bring potential practical application in water purification and energy recovery from wastewater.

© Higher Education Press 2023

1 Introduction

Growing concerns over environment degradation and energy shortage has led to increasing demand in the

✉ Corresponding author

E-mail: qhji@tsinghua.edu.cn

development of sustainable and renewable energy technologies (Liu et al., 2019). It has been proven that huge potential energy and valuable substances hid in wastewater (Lu et al., 2018). The complex set of organic pollutants can be served as carbon and energy sources for electricity generation, which are three times more than the energy required for their treatment (Zeng et al., 2020). Over the past few decades, numerous efforts based on efficient energy conversion technologies were proposed to produce electricity from wastewater at the time of degrading aqueous pollutants (Li et al., 2015; Munoz-Cupa et al., 2021).

Harvesting energy from wastewater can be realized by several technologies, such as microbial fuel cell (MFC) (Li et al., 2022), photocatalytic fuel cell (PFC) (He et al., 2022), proton exchange membrane fuel cell (PEMFC) (Wang et al., 2022), solar-driven power extraction from salinity gradient (Wang et al., 2021), and galvanic cell (Ji et al., 2019). Among these methods, PFC is one common seen successful design which utilizes solar energy as driving force and regards wastewater as substrate to convert the chemical energy of organic pollutants into electricity (Gu et al., 2021). Under light irradiation, rapid generation of electron/hole pairs would occur at photoanode and bring a fast and direct charge-transfer (Katal et al., 2021). Pollutants are oxidized and degraded by photogenerated holes, while photogenerated electrons at anode can pass through the external circuit to cathode for electricity production. In the PFC system, the photoelectrodes are very important, especially the photoanode, which could directly dominate the efficiency of photocatalytic degradation of pollutants and power generation. To date, most conventional PFC photoanodes were photocatalysts loaded on photoelectrodes. The pollutants near the anode were oxidized and a concentration gradient could be formed between the anode surfaces to bulk solution, where greatly hinder mass transfer (Li et al., 2019).

Generally, the photoanode should firstly have broadened light response and rapid electron-hole separation rate to guarantee photocatalytic performance. Secondly, it can accelerate charge transfer as it works as electron acceptor or electron buffer to carry electrons migrating from oxidized pollutants to cathode (Di et al., 2018). BiOCl is a kind of promising photoanode material because of its outstanding photocatalytic activity and it has been extensively used to degrade various refractory organic pollutants in wastewater. BiOCl has a unique layered structure interlaced with positive ($\text{Bi}_2\text{O}_2^{2+}$) and negative slabs of halogen atoms, stacked by interlayer van der Waals interactions (Zhou et al., 2018a). This open-layer structure brings enough space for related atoms and orbitals polarization and then form inherent internal static electric fields (IEF), which can greatly accelerate the separation and migration of photogenerated electron-hole pairs (Cheng et al., 2014). Since the fast and efficient

charge separation and migration is the decisive factor to superior photocatalytic efficiency (Zheng et al., 2016), numerous attempts have been made on BiOCl-based catalysts' modulation to achieve improved charge separation and suppressed recombination rate between hole/electron pairs.

Although composite BiOCl-based catalysts improve the efficiency of rapid electron/hole pair's separation, the separated photogenerated electrons need be temporary stored and migrate to cathode in minimal losses. Polyoxometalates (POMs), which are anionic metal oxide nanoclusters, have been reported as excellent electron buffers. The Keggin-type structure ($[\text{XM}_{12}\text{O}_{40}]^{n-}$ (X = P, Si, Ge; M = W, Mo, etc.)) assure its chemical stability and possibility to undergo reversible, multi-steps and multi-electron redox processes under certain conditions (Li et al., 2018). Due to the unique charge-transfer properties, POMs could benefit the photocatalytic degradation over pollutants as well as boost the activity of fuel cell (Friedl et al., 2018; Ben M'Barek et al., 2020). It has been regarded as a class of electron acceptors and carriers which can capture the electrons and store several electrons per molecule (Zu et al., 2018). Inspired by this concept, the BiOCl/POMs composites should combine the merits of both as the POMs capture the photogenerated electrons and release them onto the anode, through which the harvesting energy from wastewater can be achieved.

In this work, we synthesized BiOCl-(NH₄)₃PW₁₂O₄₀ (BiOCl-NH₄PTA) photocatalyst via two-step hydrothermal method. Air-cathode was employed as an efficient ORR cathode since oxygen could be obtained readily in air and functioned as the electron acceptor, which is conducive to power density (Zhang et al., 2017; Zhang et al., 2020). In our previous studies, we found that flow electrodes, especially flow-through structure could significantly increase the mass transfer and promote electron transfer, hence accelerate reaction kinetics (Zhou et al., 2018b; Zhou et al., 2019). Therefore, we fabricated a novel hybrid fuel cell with flow-through field (F-HFC), which combines the photocatalytic system and flow-through configuration. As a result of retarded photogenerated electrons/holes recombination time and optimized mass transfer in electrodes, enhanced performances on pollutants degradation and electricity generation (e.g., Rhodamine B (RhB), methyl orange, starch and glucose) were achieved in F-HFC. The electricity generation mechanism in the as designed F-HFC system was further elucidated. This hybrid fuel cell with flow-through field fulfills the purpose of decontamination of aqueous organic pollutants and synchronous electricity generation. It also provides insights into the rational development of photocatalysts and flow-through field structure to enhance the electron and mass transfer in water purification and energy recovery.

2 Experimental sections

2.1 Chemicals and materials

Bismuth nitrate pentahydrate ($\text{Bi}(\text{NO}_3)_3 \cdot 5\text{H}_2\text{O}$), polyvinylpyrrolidone (PVP), mannitol ($\text{C}_6\text{H}_{14}\text{O}_6$), tungstophosphoric acid ($\text{H}_3\text{PW}_{12}\text{O}_{40}$), ammonium chloride (NH_4Cl), sodium chloride (NaCl), RhB, methyl orange (MO), starch, glucose, sodium sulfate (Na_2SO_4) were purchased from Sigma Aldrich (Shanghai, China). All chemicals used in the experiments were analytical grade and solutions were prepared using ultrapure water ($18.2 \text{ M}\Omega\cdot\text{cm}$) (Milli-Q Advantage, Merck Millipore, Germany).

2.2 Catalysts preparation

The synthesis of $(\text{NH}_4)_3\text{PW}_{12}\text{O}_{40}$ (namely NH₄PTA) catalyst was prepared based on our previous research. Briefly, $\text{H}_3\text{PW}_{12}\text{O}_{40}$ (300 mg, 0.1 mmol) and NH₄Cl (27 mg, 0.5 mmol) was dissolved in 20 mL and 10 mL water, respectively. The molar ratio of NH₄Cl to $\text{H}_3\text{PW}_{12}\text{O}_{40}$ was 5:1. The as prepared NH₄Cl solution was then slowly drop wise into $\text{H}_3\text{PW}_{12}\text{O}_{40}$ solution and stirred for 10 min. The above mixture was transferred into a 50 mL Teflon-lined stainless steel autoclave and heated at 140 °C for 12 h. After naturally cooled down to the room temperature, the solid powder was collected by centrifugation and washed with ultrapure water for several times to remove excess ions, and then freeze-dried for overnight.

The synthesis of BiOCl-(NH₄)₃PW₁₂O₄₀ (namely BiOCl-NH₄PTA) catalyst was obtained by two-step hydrothermal method. Firstly, the BiOCl catalyst was prepared according to Guan et al. (2013). Briefly, 486 mg Bi(NO_3)₃·5H₂O and 400 mg PVP were dissolved in 25 mL 0.1 mol/L mannitol solution and facilitated by ultrasound or vigorous magnetic stirring. Then, 5 mL of saturated NaCl solution was slowly added dropwise into the solution and yield a uniform white suspension. After 10 min agitation, a certain amount of as-obtained NH₄PTA was added into the mixture and then transferred into a 50 mL Teflon-lined stainless steel autoclave and heated at 140 °C for 3 h. After cooled down to the room temperature, the obtained white solid was collected by centrifugation and washed with ultrapure water for several times to remove residual ions, and then freeze-dried for overnight.

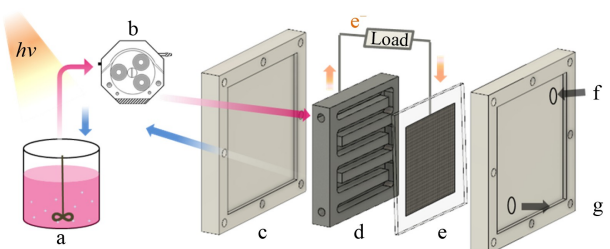
2.3 Assembly of hybrid fuel cell with flow-through field

The commercialized membrane electrode assembly (MEA) was purchased from XingQiao, Co. Ltd., China. The MEA was composed of a Nafion membrane in the middle, a carbon paper with Pt/C catalyst loaded (0.7 mg/cm²) on one side and a carbon paper with Pt/C catalyst loaded (0.2 mg/cm²) on the other side. The

carbon paper with 0.2 mg/cm² Pt/C catalysts was pressed against a graphite flow-through field collector, which has a serpentine groove in 5 mm wide, 5 mm deep and 11 cm long (5.5 cm² projected areas) and functioned as anode. The carbon paper with 0.7 mg/cm² Pt/C catalysts loaded was used as air cathode. The whole component was then clamped between two fixture fabricated acrylic glass end plates as shown in Scheme 1, and the practical photo of the components were provided in Fig. S1. In the experiment, the solution with added photocatalysts were pumped from the beaker into the anode reaction cell and then flowed back to the beaker. Meanwhile, oxygen was purged through the cathode cell at a flow rate of 20 mL/min. The temperature of the solution was maintained around 25 °C (room temperature) by the water bath. The solution flow rate through the anode graphite reactor was 16 mL/min. The hybrid fuel cell was connected to a Gamry Interface 1000 electrochemical workstation.

2.4 Photocatalytic degradation experiment

The photocatalytic performance of as-synthesized catalysts were evaluated by degrading Rhodamine (RhB) under simulated solar irradiation at ambient temperature using a 500 W Xe lamp (CEL-S500, CEAULIGHT, China) and the light intensity was calibrated to 100 mW/cm². Photo-degradation over methyl orange (MO), starch, and glucose were also investigated. In the experiment, 30 mg catalysts were added into 40 mL RhB solution with the initial RhB concentration of 30 mg/L. The solution initial pH was adjusted to 5.0 ± 0.1 by 0.5 mol/L NaOH and 0.1 mol/L H₃PO₄ solution. A magnetic stirrer was used to agitate the solution at 300 r/min unless otherwise mentioned. Prior to irradiation, the suspension was magnetically stirred for 30 min in the dark to achieve the adsorption/desorption equilibrium. And then the solution was irradiated for a certain time with a distance of 15 cm from the solution surface to the lamp. After irradiated for a certain time, samples were taken from the solution at predetermined intervals and centrifuged at 5000 r/min to remove the remaining particles and then diluted for test.



Scheme 1 Schematic diagrams of the hybrid cell (a) transparent beaker with RhB-photocatalyst; (b) peristaltic pump; (c) acrylic plastic end plate for seal; (d) graphite electrode with flow-through field; (e) MEA (Nafion 117 polymer exchange membrane and air-cathode); (f) oxygen inlet; (g) water and oxygen outlet.

The RhB concentration was detected by UV-vis spectrophotometer. The removal efficiency of pollutants was calculated by C/C_0 , and the degradation kinetics were calculated by $\ln(C - C_0) = -kt$, where k (min^{-1}) is the rate constant; C_0 and C (mg/L) are the initial concentration and the concentration at irradiated time interval t (min), respectively.

2.5 (Photo)electrochemical measurements

The transient photocurrent characterization was carried out in a quartz cell on a CHI660 electrochemical workstation in three-electrode system. The BiOCl and composite BiOCl-NH₄PTA were dissolved in the ethanol and Nafion solution. The mixtures were then painted on planar F-doped tin oxide (FTO) substrate. Detailed information was provided in Supporting Materials. The BiOCl/FTO or BiOCl-NH₄PTA/FTO conductor glass, Ag/AgCl electrode, and the platinum wire were used as the working, reference and counter electrode, respectively. Na₂SO₄ (0.1 mol/L) was used as electrolyte. The photocurrent–voltage curves were measured at a scan rate of 10 mV/s. The current density–voltage (J - V) curves of the fuel cell were collected on a Gamry electrochemical workstation, where the graphite collector and air-cathode were used as working and counter electrode, respectively.

2.6 Characterization

The morphology of catalysts was characterized by field-emission scanning electron microscopy (SEM, SU8020, Hitachi, Japan) and high-resolution transmission electron microscopy (HRTEM, JEM-2100F, JEOL, Japan) coupled with an energy dispersive X-ray spectroscopy (EDS). X-ray powder diffraction (XRD) patterns were obtained with an X’Pert PRO Powder diffractometer (X’Pert Pro, PANalytical, Netherlands) with a copper K α source, monitoring in the range from $2\theta=5^\circ$ to 90° at a scan rate of $5^\circ/\text{min}$. The RhB and MO concentration was measured by a UV-vis spectrophotometer (U-3900, Hitachi, Japan) at 554 nm and 466 nm respectively after centrifuged. The starch and glucose degradation were analyzed by total organic carbon (TOC) using TOC measuring instrument (TOC-L, Shimadzu, Japan). The UV-vis diffuse reflectance spectra (DRS) were achieved by a spectrophotometer (Lambda 650, PerkinElmer, China) and BaSO₄ was used as the reflectance sample. The steady-state fluorescence and time-resolved fluorescence spectra were obtained using a fluorescence spectrometer (FLS 980, Edinburgh Instruments Ltd., UK) with excitation at 395 nm. The (photo) electrochemical measurements were measured on electrochemical workstation (Interface 1000, Gamry, USA; CHI 660, Chenhua, China). The band gap energy can be calculated based on the following Tauc plot formula by extrapolating the straight portion of $(ahv)^{0.5}$ against the hv

plot to $\alpha = 0$ (Eq. (1)).

$$\alpha h\nu = A(h\nu E_g)^{n/2}, \quad (1)$$

where α , h , v , A and E_g are the absorption coefficient, Planck’s constant, the light frequency, a constant and the band gap, respectively (Vadivel et al., 2016).

3 Results and discussion

3.1 Characterization of photocatalytic catalysts

The morphologies of pure BiOCl, NH₄PTA and BiOCl-NH₄PTA composite were characterized by SEM and shown in Figs. 1(a)–1(c). It can be observed that the BiOCl obtained by hydrothermal method possesses plate-like structure while the pure NH₄PTA were sphere-shaped nanoparticles with diameter of ~400 nm. However, there were no clear boundaries nor obvious specific shapes could be found in the BiOCl-NH₄PTA composite. The morphology of catalysts was further investigated by HRTEM and presented in Figs. 1(e)–1(h). As shown in Fig. 1(e), the BiOCl was uniformly distributed ultrathin nanoplates. Compared to the pure spherical NH₄PTA with the smooth surface, the edge was much rougher in the BiOCl-NH₄PTA composite. Local magnification of the composite edges in Fig. 1(h) revealed that the ultrathin BiOCl nanoplates were on the surface of NH₄PTA spheres, which looks like small tentacles. These BiOCl small tentacles on the surface of NH₄PTA sphere could not only inhibit BiOCl nanosheets overlapped and agglomeration, but also expose more active sites (Xu et al., 2014; Shen et al., 2021). The EDS mapping analysis on Bi, W, P and Cl elements were carried out and shown in Fig. 1(i). The distributions of the four elements’ signals in the composites were uniform. The areas of Bi and Cl signal were larger than that of P and W signal, which indicating the successful combination of highly dispersed BiOCl onto the surface of NH₄PTA spheres.

The crystallinity and phase purity of the prepared catalysts were identified by powder XRD patterns. As shown in Fig. 1(d), all the diffraction peaks in BiOCl catalysts fit well with tetragonal BiOCl (JCPDS 82-0485). The diffraction peaks at 12.03° , 25.91° , 32.55° , and 33.52° were indexed to (001), (101), (110), and (102) reflections, respectively. The relative enhanced peak intensity at 32.55° reveals the preferential orientation of the crystalline plan (110) in the BiOCl catalysts. Sharp peaks could be observed in NH₄PTA catalyst which suggests that small particles were formed. The diffraction peaks were well indexed to JCPDS 50-0305 and no traces of other phases were discovered, which indicates the presence of pure crystalline Keggin-type structure POM. The diffraction peaks observed in the as-synthesized BiOCl-NH₄PTA composite were majorly possessed the

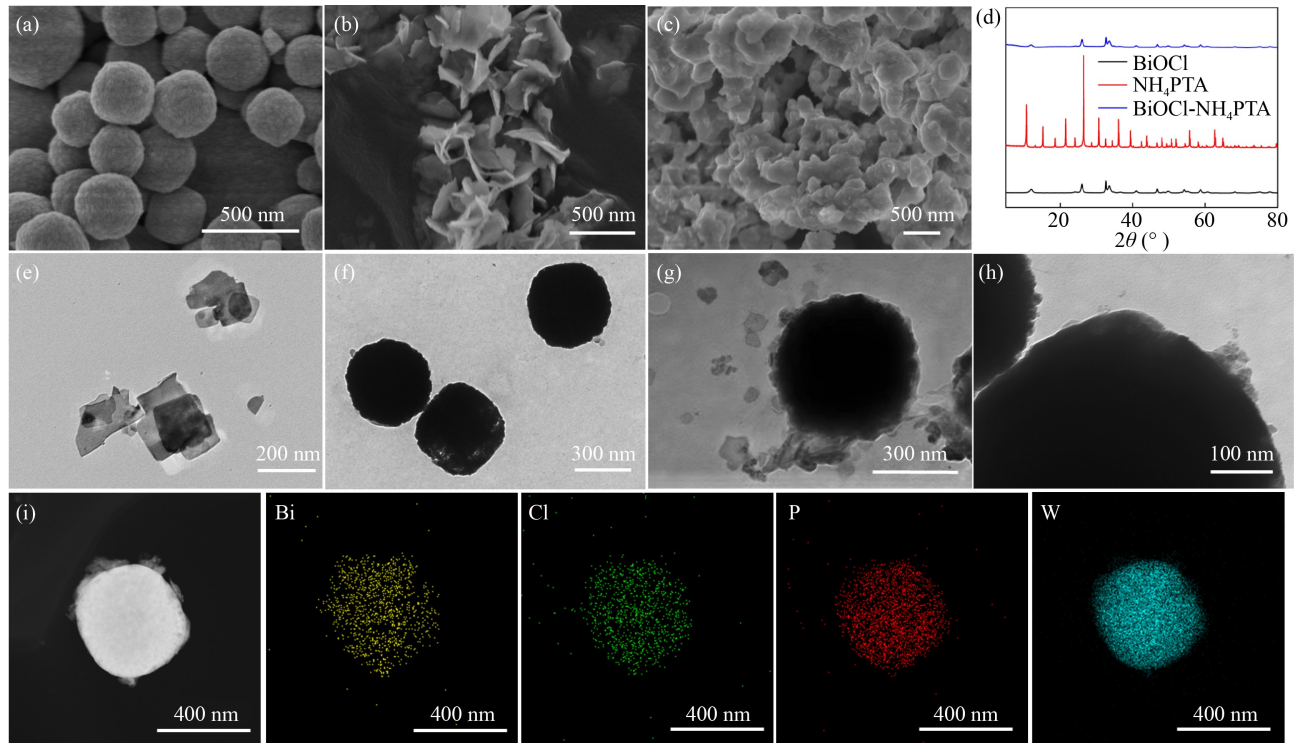


Fig. 1 Materials characterization. High magnification SEM images of (a) BiOCl, (b) NH₄PTA, (c) BiOCl-NH₄PTA; (d) XRD patterns of BiOCl, NH₄PTA and BiOCl-NH₄PTA; HRTEM images of (e) BiOCl, (f) NH₄PTA, (g) BiOCl-NH₄PTA, (h) higher magnification of BiOCl-NH₄PTA; (i) the TEM image and EDS mapping of Bi, Cl, P, W elements of BiOCl-NH₄PTA.

pure BiOCl peaks while the intensity of NH₄PTA peaks were relatively weak. Very similar results were previously reported by Ito et al. (2001). It was supposed that when the BiOCl nanosheets attached on the surface of NH₄PTA spheres, good coverage brought by uniformly attachments as well as lower content of NH₄PTA spheres may contribute to this.

3.2 Photocatalytic performance measurements of BiOCl-NH₄PTA

The photocatalytic degradation of organic dyes or other toxic pollutants was of great importance to the water remediation while the removal efficiency is the intuitive index to evaluate the activity of photocatalysts. To evaluate the performance of BiOCl-NH₄PTA in water decontamination, RhB was chosen as the model pollutants. By changing the amounts of NH₄PTA and BiOCl, a series of BiOCl-NH₄PTA composites with different Bi to W ratios were obtained. After 30 min stirring in dark, the photocatalytic experiments started after 30 min stirring in dark to reach the absorption equilibrium and exclude its effect on pollutants removal. The concentration of RhB was slightly decreased which indicated that the catalysts have limited absorption ability over dyes. The representative kinetic plots of RhB degradation by single catalysts and different ratios of Bi to W in composite catalysts were shown in Fig. 2(a).

During the irradiation process, the pure NH₄PTA had negligible photocatalytic ability while pure BiOCl could degrade the dyes to a certain extent, with the degradation kinetic increased from 0.0005 to 0.0151 min⁻¹ and around 67.5 % dyes were removed in 60 min. Although the NH₄PTA has scarcely catalytic capability, the BiOCl-NH₄PTA composites could greatly promote the catalytic performance compared to pure BiOCl catalysts. The influence of Bi to W ratios on pollutants degradation performance was studied. In the ratios of 1:0.25 (Bi:W) composite catalysts, the RhB degradation kinetics was improved by 34.4 % and the kinetics increased successively with the increasing ratios of Bi to W from 1:0.25 to 1:1. The best performance could be found in ratios of 1:1 since 86.7 % of dyes were degraded in 30 min irradiation, and all dyes were nearly fully removed within 90 min. The photocatalytic ability was boosted and the degradation kinetics constant was 3.2 times faster than that of pure BiOCl, rising from 0.0151 to 0.0636 min⁻¹. However, further increase the Bi to W ratios to 1:2 resulted in a decrease in photocatalytic degradation activity. The appropriate ratio of BiOCl and NH₄PTA would benefit synergistic effect and the ratio of 1:1 was optimized and selected for the following experiments.

The operational parameters could greatly affect the photocatalytic performance. Herein, the influences of solution pH value, catalysts dosage, initial concentration, and the flow rate were further investigated. A broad range

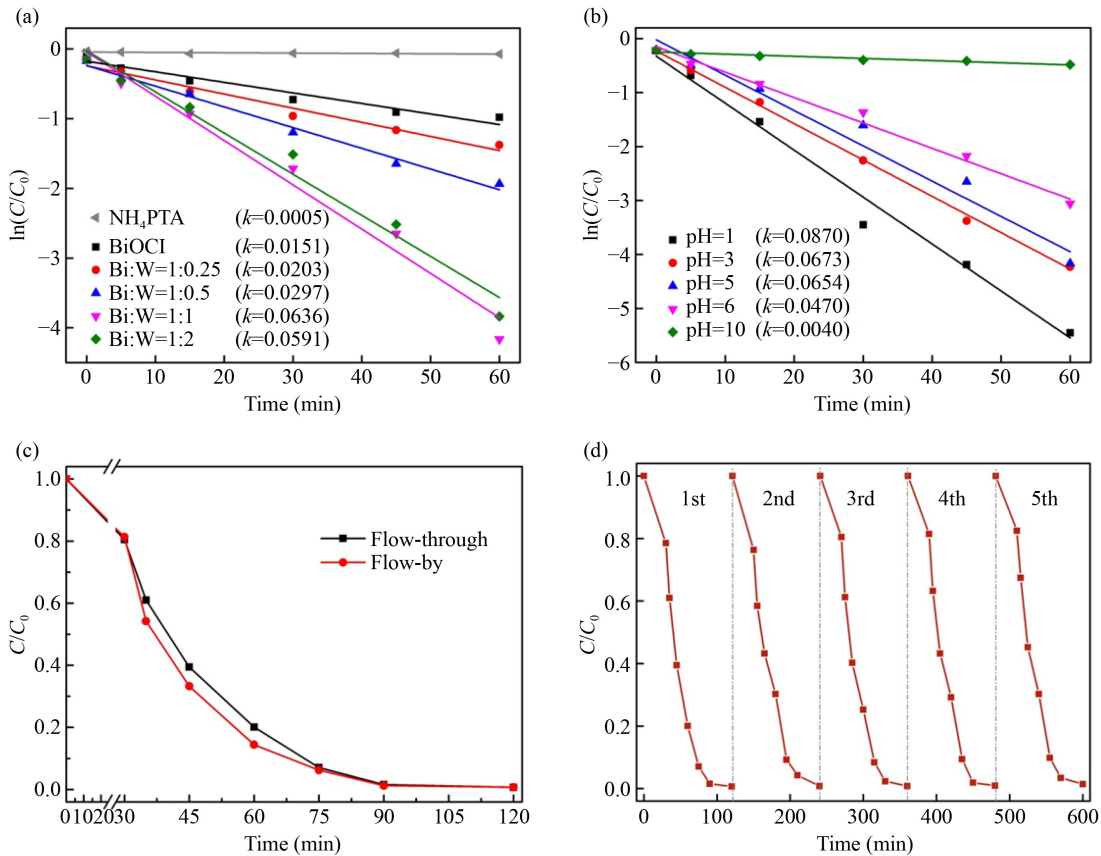


Fig. 2 Photocatalytic performances of the BiOCl-NH₄PTA. Kinetic investigation of RhB photocatalytic degradation by (a) BiOCl-NH₄PTA composite with different Bi: W ratios, (b) BiOCl-NH₄PTA under different pH condition; (c) photocatalytic performances of BiOCl-NH₄PTA in flow-through field and immersed configuration; (d) investigation on stability test on photo-degradation efficiency of RhB for five cycles.

of pH value from 1 to 10 was studied in the photocatalytic degradation process and shown in Fig. 2(b). The photocatalytic kinetic constant reached the highest value to 0.0870 min^{-1} at the pH 1 and then dropped with the increase of pH values. The kinetic constant decreased to 0.0040 min^{-1} at pH 10 and only 39.7 % pollutants could be degraded in the alkaline condition. The pH value before and after the experiments were measured and the change were within ± 0.2 . Since the surface charge of catalyst was positive in acidic condition, photo-generated electrons were tending to migrate to catalyst's surface, which was in favor of the rapid separation of photogenerated-hole/electron pairs and then facilitate photocatalytic reaction. Furthermore, the electrons may combine with the molecular oxygen to generate super oxide radicals, which could greatly accelerate the photocatalytic rates. As shown in Fig. S2, higher dosage of catalysts and lower initial concentration of RhB led to faster photocatalytic rates (Zhang et al., 2009; Cui et al., 2013).

In the hybrid fuel cell, the RhB solution with the BiOCl-NH₄PTA was pumped through the anode cell. The details of cell fabrication were provided in Fig. S3 and the

corresponding photo-degradation efficiency over RhB were shown in Fig. 2(c). Compared to traditional immersed configuration, the temporary darkness in the serpentine grooves would slightly decrease pollutants' degradation efficiency. However, due to the unique properties of POMs and the optimal control of flow rates, the negative impacts were quite small relative to the fast RhB degradation rates, which could be ignored. The durability and stability of BiOCl-NH₄PTA were also investigated in recycling experiments for RhB photo-degradation. As shown in Fig. 2(d), the photo-degradation efficiency remains high after five cycles, suggesting that the as-prepared photo-catalyst was stable under long time irradiation, which was great important for practical application.

3.3 The electricity generation performance of the BiOCl-NH₄PTA in F-HFC system

In the F-HFC system, the influence of solution flow rate was studied. Flow rate was expected to be as high as possible so that the solution could move quickly into the conductive graphite collector to complete the photo-

electricity conversion process. Higher flow rate could facilitate the mass transport (Parmar et al., 2015). The maximum flow rate in the experiment was set as 27 mL/min to ensure the reactor remained at steady state. As shown in Fig. 3(a), the photocatalytic kinetic values were negatively correlated to flow rate. Nevertheless, the difference of kinetic constant is relatively small and flow rate had limited effect on the photocatalytic rate in this F-HFC system. It is speculated that lower flow rate brings more retention time and allows the catalysts exposed to

irradiation for longer. In the experiment, dyes and other natural polymeric biomass, such as starch and glucose were also selected as model pollutants to evaluate the performance of the F-HFC. As shown in Fig. 3(b), 91.8 % methyl orange was discolored in 45 min and fully degraded in 60 min. The starch and glucose could also be oxidized and degraded to starch oligomers and glucose derivatives under light irradiation, with degradation efficiency of 57.1 % and 83.8 % in 120 min, respectively.

The electricity generation performance in F-HFC

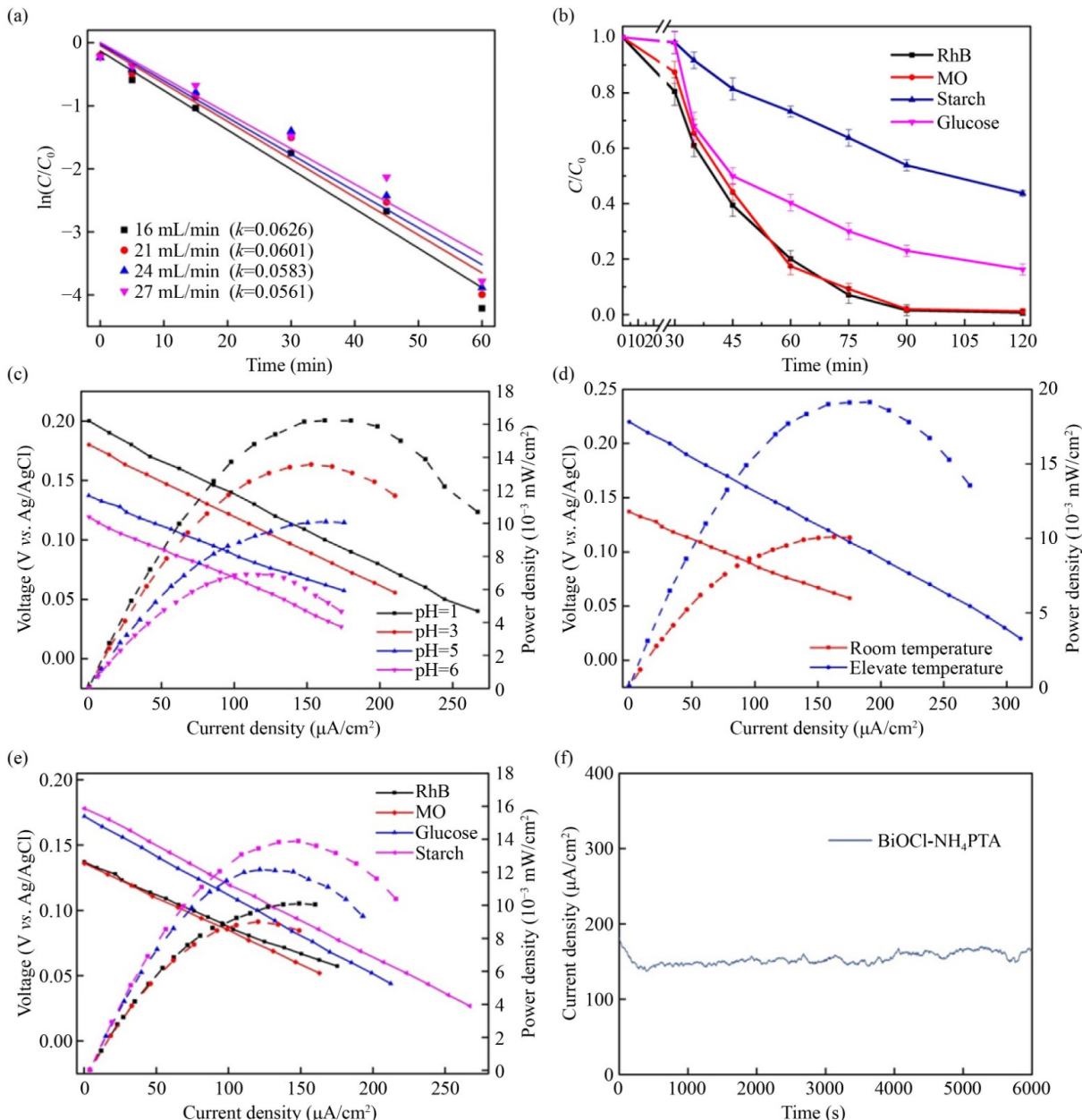


Fig. 3 The electricity generation performance of the BiOCl-NH₄PTA in F-HFC system. (a) Kinetic investigation of RhB photocatalytic degradation under different flow rates; (b) photocatalytic degradation efficiency of different targeted pollutants; (c) voltage–current density and power–current density plots with different pH at room temperature; (d) voltage–current density and power–current density plots at elevated temperature (80 °C); (e) voltage density and power–current density plots with different pollutants; (f) current density of F-HFC system (Initial RhB concentration is 30 mg/L, flow rate is 16 mL/min).

system was investigated. In the experiment, 30 mg/L RhB solution was mixed with BiOCl-NH₄PTA in the beaker and pumped through the anode graphite collector. The oxygen was purged into the air-cathode. Considering the large energy difference between ORR onset potential on Pd/C air cathode and the conduction band of BiOCl, the photogenerated electrons in the BiOCl-NH₄PTA catalysts would migrate to the air-cathode spontaneously and leaving the photogenerated holes for oxidation reactions (Gu et al., 2021). Therefore, the electricity output could be easily collected from the external circuit in the F-HFC system. The voltage-current density and power-current density curves of RhB under different pH values were measured and showed in Fig. 3(c). It can be observed that the pH value greatly affect the power output density. At the extremely acidic condition at pH 1, a short-circuit current density of ~267.1 μA/cm² and maximum power density (P_{max}) of ~16.2 μW/cm² were measured. The current density declines as the pH increases, and the current density was 175.3 μA/cm² with power density reached to ~10.1 μW/cm². The electricity production of the fuel cell should be owing to the photocatalytic degradation at the photocatalysts and the tendency of electricity generation was coincided well with the photodegradation efficiency under different pH conditions. The lower pH condition facilitates the RhB degradation as well as the acidic condition was conducive to the F-HFC electric power output. The anodic solution was placed under irradiation and heated to 80 °C at the same time. The current density and the maximum power density were increased to 270.9 μA/cm² and 19.1 μW/cm² (Fig. 3(d)) respectively, when the anodic solution temperature elevated to 80 °C. The elevated temperature could benefit the POM in composite catalysts discharging at the cathode which leads to higher power output. And it was proven that the change of solution pH coupled with thermal effect could directly affect the POM' redox condition and the charge transfer capability of electrons (Liu et al., 2014a). As summarized in Table S1, this F-HFC revealed enhanced photoelectrical conversion performance compared to other work which employing BiOCl-based as photoanode in PFC system. The performance of F-HFC powered by various pollutants was also examined and shown in Fig. 3(e). The power densities were 9.0 μW/cm², 12.2 μW/cm², and 13.9 μW/cm², respectively, when MO, glucose and starch used as substrates. The chemical energy in dyes and biomass could be extracted and converted directly for electricity generation without pretreatment. Simplified pre-treatment process makes it more practical and economic, and its adaptation to more kinds of pollutants indicates this F-HFC system has a broader scope of potential application.

The discharged current densities in the F-HFC system were measured under different conditions. When no photocatalysts, pollutants or irradiation, almost no current were generated in the system and the discharged current

density were extremely low (Fig. S4). In comparison, the discharged current density was measured in the operation of the hybrid cell driven by RhB under the irradiation. During the whole discharge period, the current remained stable and the current density reached up to 180 μA/cm² (Fig. 3(f)). The durability test of the BiOCl-NH₄PTA catalyst and the stable current curves observed revealed its possibility use for long-time practical application.

3.4 Mechanism study

The mechanism of enhanced photocatalytic performance and electricity generation brought by composite catalysts were studied. The UV/Vis diffuse reflection spectra (DRS) were performed to explore the optical properties of the as-prepared catalysts. As shown in the Fig. 4(a), the adsorption edge of pure BiOCl was lower than ~320 nm. The band gap edge of the absorption was relatively red-shifted in BiOCl-NH₄PTA composite with respect to the pure BiOCl. It indicated that BiOCl-NH₄PTA catalyst broadened the absorption of visible region, thus more light could be utilized and thus benefit photocatalytic degradation efficiency. The extended photo-response range could be ascribed to the changes of band gap, which were further calculated based on the Tauc plot formula and shown in Fig. 4(b). The calculated band gap energies of BiOCl and BiOCl-NH₄PTA were 3.02 eV and 2.11 eV, respectively. The reduction of band gap width referred to wider extended wavelength range for photocatalytic reaction process.

Efficient charge separation and transfer are vital to the photocatalytic efficiency and can be verified by transient photocurrent responses. As shown in the Fig. 4(c), both pure BiOCl and BiOCl-NH₄PTA could produce photocurrent under the irradiation. In the pure BiOCl, the value of photocurrent was quite low. Comparatively, the photocurrent in BiOCl-NH₄PTA was greatly enhanced and reached to 5 μA/cm². It suggested that much more electrons were effectively generated and transferred on the surface of the BiOCl-NH₄PTA photocatalysts. To further confirm the enhancement of charge carrier separation efficiency, the analyses of charge carrier lifetime were performed by the time-resolved fluorescence emission decay spectra (Wang et al., 2018) and shown in Fig. 4(d). The emission decay curves could be fitted well to a triexponential function and the fitting parameters were summarized in Table S2. The intensity-average lifetimes were calculated to be 1.28 ns and 3.43 ns for BiOCl and BiOCl-NH₄PTA, respectively. The longer lifetime found in BiOCl-NH₄PTA proved that the existence of polyoxometalates could retard the recombination time of photo-generated electrons and holes, and lead to superior charge separation efficiency. As discussed before, the BiOCl-NH₄PTA composite has morphology of ultrathin BiOCl nanosheets attached on the surface of NH₄PTA shperes. Upon irradiation, the

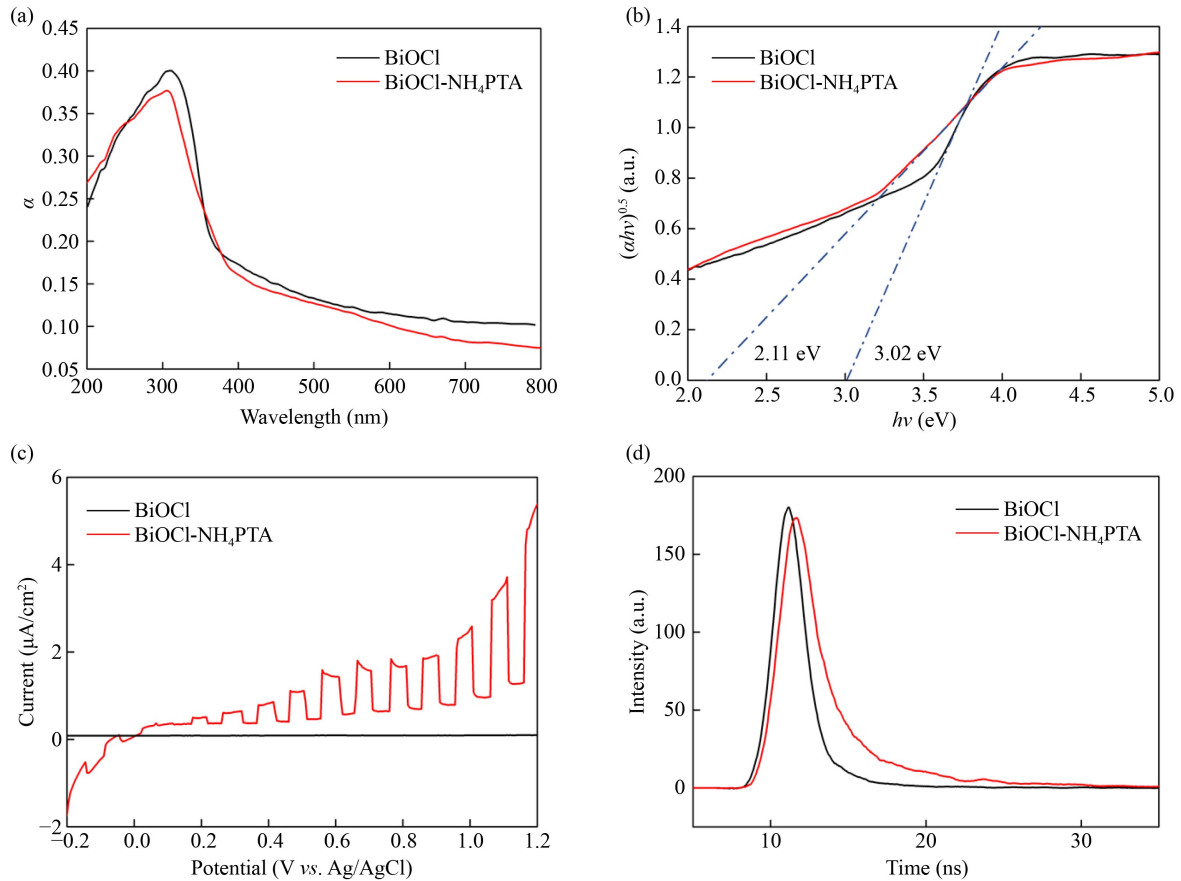


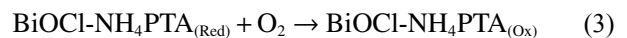
Fig. 4 (a) UV-vis diffuse reflection spectra of BiOCl and BiOCl-NH₄PTA; (b) The Tauc plot of BiOCl and BiOCl-NH₄PTA; (c) Transient photocurrent curves of BiOCl and BiOCl-NH₄PTA; (d) Photoluminescence spectra of BiOCl and BiOCl-NH₄PTA.

BiOCl nanosheets could efficiently absorb light and many electron-hole pairs were generated rapidly. As NH₄PTA were electron acceptors and carriers, the electrons on the BiOCl were supposed to be captured by the NH₄PTA spheres, leaving holes on BiOCl surfaces, which effectively retard the electron/holes recombination time.

Apart from lengthening the recombination time, as a class of POM, the redox state of NH₄PTA would change due to its ability of undergoing reversible multi-electron process (Symes and Cronin, 2013; Liu et al., 2020). The XPS measurement was performed in order to clarify the valence states and electronic structure of W atoms in BiOCl-NH₄PTA (Fig. S5). Before the irradiation, two peaks at the binding energies of 35.90 eV and 38.05 eV could be observed, which correspond to W 4f(7/2) and W 4f(5/2) and were attributed to W⁶⁺ state (Jalil et al., 2003). After 2 hours irradiation, the binding energies were shifted toward lower values to 35.35 eV and 37.50 eV respectively. Meanwhile, the two peaks were divided into smaller ones at 33.8 eV and 36.93 eV, which corresponds to W⁵⁺ state (Naseri et al., 2011; Mohamed et al., 2019). The slightly negative shift of peaks indicate that the chemical environment of W turns into higher electronegativity after accepting photoelectrons and the oxidation

state of W atoms was partly changed into lower valence (Rengifo-Herrera et al., 2016).

Based on the XPS analysis and literature, at first, POMs remained in oxidation state POM_(Ox) and its redox potential was high enough for dyes and biomass oxidation (Song and Bartea, 2004). The POMs would oxidize the pollutants and itself was reduced to reduced form POM_(Red) (Yang et al., 2019b). Then, the POM_(Red) was readily regenerated by oxygen under mild conditions to POM_(Ox) that have been proven by previous studies (Yang et al., 2019a). Herein, the half-cell reaction using BiOCl-NH₄PTA in the anode could be represented into two major steps (Eqs. (2) and (3)).



Meanwhile, the oxygen reduction reaction occurred at air cathode. As the result, the net reaction of the F-HFC is oxidation of dyes or biomass to produce electricity. The ORR activity of air-cathode was evaluated using linear sweep voltammetry (Fig. S6) and an onset potential of 0.895 V (vs. RHE) was achieved. The redox potential of BiOCl-NH₄PTA was important to determine whether the

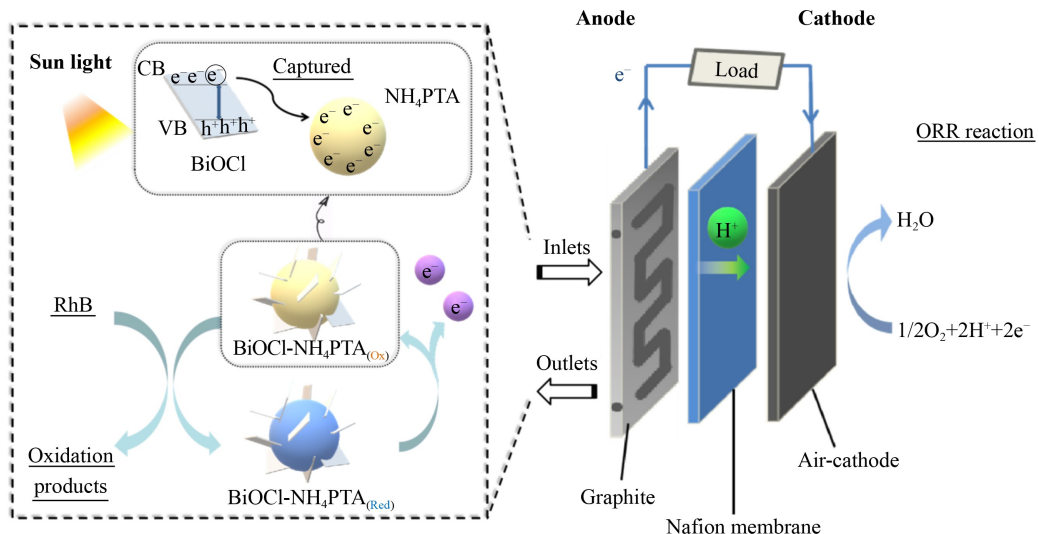


Fig. 5 Schematic illustration of the hybrid F-HFC.

fuel cell could function properly. The higher standard redox potential brought greater tendency to oxidize the pollutants but lower the tendency to be oxidized by oxygen (Liu et al., 2014b). The reduction potential for $\text{BiOCl}-\text{NH}_4\text{PTA}_{(\text{Red})}$ was determined to be 0.351V (vs. RHE) (Sadkane and Steckhan, 1998). Herein, the reduced $\text{BiOCl}-\text{NH}_4\text{PTA}$ release electrons on the graphite collector anode to air-cathode spontaneously and an electricity output can be collected from the external circuit. The $\text{BiOCl}-\text{NH}_4\text{PTA}_{(\text{Red})}$ could then be regenerated by oxygen oxidation because of the lower potential compared to oxygen (1.23 V vs. NHE) (Liu et al., 2014a).

The principal diagram of the F-HFC for improving decontamination of aqueous organic pollutants and synchronous electricity generation was shown in Fig. 5. Under the light irradiation, electron/hole pairs were rapidly generated in BiOCl nanosheets in $\text{BiOCl}-\text{NH}_4\text{PTA}$ composites. The photogenerated holes were strong oxidants towards the dyes and biomasses. Meanwhile, the photogenerated electrons could transfer from BiOCl to NH_4PTA spheres and temporary stored in NH_4PTA . The retarded recombination time of photogenerated electrons/holes pairs greatly accelerate the photocatalytic degradation rates. In the F-HFC system, the $\text{BiOCl}-\text{NH}_4\text{PTA}$ and pollutants were pumped cyclically through the graphite collector and the graphite collector functioned as anode. Upon photocatalytic oxidizing pollutants, the $\text{BiOCl}-\text{NH}_4\text{PTA}$ in originally oxidative state $\text{BiOCl}-\text{NH}_4\text{PTA}_{(\text{Ox})}$ captured electrons and itself would be reduced to $\text{BiOCl}-\text{NH}_4\text{PTA}_{(\text{Red})}$. $\text{BiOCl}-\text{NH}_4\text{PTA}_{(\text{Red})}$ could then be oxidized by oxygen and turn back to oxidized form and be regenerated. At air cathode, the oxygen reduction reaction occurred. Herein, the electricity was produced with water decontaminated simultaneously. Notably, the pollutants degradation was in the beaker by photocatalytic process, while the output

of electricity happened in the flow-through reactor. The separation of photodegradation unit and electricity generation unit were realized.

4 Conclusions

In summary, we demonstrated a novel flow-through fuel cell using $\text{BiOCl}-\text{NH}_4\text{PTA}$ composites as photocatalysts and electron carriers. As NH_4PTA functioned as an electron acceptor and buffer, the as-prepared $\text{BiOCl}-\text{NH}_4\text{PTA}$ composite have enhancement on photocatalytic oxidization ability over pollutants as well as power outputs compared to pure photocatalysts BiOCl . The novel fabricated F-HFC was the hybrid of photocatalytic system and flow-through field configuration which could strength the merits of both to effectively extract the potential chemical energy in the aqueous pollutants. Unlike the fuel cell which needs harsh operation conditions (MFC) or can not directly utilize wastewater as substrate (PEMFC), this novel abiotically catalyzed fuel cell could run under a wider pH range, low temperature (room temperature), and directly convert dyes and biomass without pretreatment for electricity generation. Since the photodegradation unit and the electricity generation unit were separated in space, the F-HFC was promising for practical large scale application. We expect that the present work will promote the design of high-performance photocatalysts coupled with fuel cell system with flow-through field to provide a new solution to environmental treatment and energy recovery simultaneously.

Acknowledgements This work was supported by the National Natural Science Foundation of China (Nos. 51738013, 52022048 and 51978371) and the Excellent Innovation Project of Research Center for Eco-Environmental Sciences (No. CAS RCEES-EEI-2019-02).

Electronic Supplementary Material Supplementary material is available in the online version of this article at <https://doi.org/10.1007/s11783-023-1611-6> and is accessible for authorized users.

References

- Ben M'Barek Y, Rosser T, Sum J, Blanchard S, Volatron F, Izzet G, Salles R, Fize J, Koepf M, Chavarotp-Kerlidou M, et al. (2020). Dye-sensitized photocathodes: boosting photoelectrochemical performances with polyoxometalate electron transfer mediators. *ACS Applied Energy Materials*, 3(1): 163–169
- Cheng H, Huang B, Dai Y (2014). Engineering BiOX (X = Cl, Br, I) nanostructures for highly efficient photocatalytic applications. *Nanoscale*, 6(4): 2009–2026
- Cui W, Wang H, Liang Y, Han B, Liu L, Hu J (2013). Microwave-assisted synthesis of Ag@AgBr-intercalated K₄Nb₆O₁₇ composite and enhanced photocatalytic degradation of Rhodamine B under visible light. *Chemical Engineering Journal*, 230: 10–18
- Di J, Chen C, Zhu C, Ji M, Xia J, Yan C, Hao W, Li S, Li H, Liu Z (2018). Bismuth vacancy mediated single unit cell Bi₂WO₆ nanosheets for boosting photocatalytic oxygen evolution. *Applied Catalysis B: Environmental*, 238: 119–125
- Friedl J, Holland-Cunz M V, Cording F, Pfanschilling F L, Wills C, McFarlane W, Schricker B, Fleck R, Wolfschmidt H, Stimming U (2018). Asymmetric polyoxometalate electrolytes for advanced redox flow batteries. *Energy & Environmental Science*, 11(10): 3010–3018
- Gu Z A, Zhou J, An X Q, Chen Q, Hu C Z, Liu H J, Qu J H (2021). A dual-biomimetic photocatalytic fuel cell for efficient electricity generation from degradation of refractory organic pollutants. *Applied Catalysis B: Environmental*, 298: 120501–120511
- Guan M, Xiao C, Zhang J, Fan S, An R, Cheng Q, Xie J, Zhou M, Ye B, Xie Y (2013). Vacancy associates promoting solar-driven photocatalytic activity of ultrathin bismuth oxychloride nanosheets. *Journal of the American Chemical Society*, 135(28): 10411–10417
- He Y, Chen K D, Leung M K H, Zhang Y Z, Li L, Li G S, Xuan J, Li J F (2022). Photocatalytic fuel cell: a review. *Chemical Engineering Journal*, 428: 131074–131092
- Ito T, Inumaru K, Misra M (2001). Epitaxially self assembled aggregates of polyoxotungstate nanocrystallites, (NH₄)₃PW₁₂O₄₀: synthesis by homogeneous precipitation using decomposition of urea. *Chemistry of Materials*, 13(3): 824–831
- Jalil P A, Faiz M, Tabet M, Hamdan N M, Hussain Z (2003). A study of the stability of tungstophosphoric acid, H₃PW₁₂O₄₀, using synchrotron XPS, XANES, hexane cracking, XRD, and IR spectroscopy. *Journal of Catalysis*, 217(2): 292–297
- Ji Q, Zhang G, Liu H, Liu R, Qu J (2019). Field-enhanced nanoconvection accelerated electrocatalytic conversion of water contaminants and electricity generation. *Environmental Science & Technology*, 53(5): 2713–2719
- Katal R, Tanhaei M, Hu J Y (2021). Photocatalytic degradation of the acetaminophen by nanocrystal-engineered TiO₂ thin film in batch and continuous system. *Frontiers of Environmental Science & Engineering*, 15(2): 27
- Li C, Feng Y, Liang D, Zhang L, Tian Y, Yadav R S, He W (2022). Spatial-type skeleton induced *Geobacter* enrichment and tailored bio-capacitance of electroactive bioanode for efficient electron transfer in microbial fuel cells. *Science of the Total Environment*, 821: 153123–153134
- Li M, Liu Y, Dong L, Shen C, Li F, Huang M, Ma C, Yang B, An X, Sand W (2019). Recent advances on photocatalytic fuel cell for environmental applications: the marriage of photocatalysis and fuel cells. *Science of the Total Environment*, 668: 966–978
- Li Q Y, Zhang L, Dai L, Tang H, Li Q, Xue H G, Pang H (2018). Polyoxometalate-based materials for advanced electrochemical energy conversion and storage. *Chemical Engineering Journal*, 351: 441–461
- Li W W, Yu H Q, Rittmann B E (2015). Chemistry: reuse water pollutants. *Nature*, 528(7580): 29–31
- Liu M, Wang L, Zhao K, Shi S, Shao Q, Zhang L, Sun X, Zhao Y, Zhang J (2019). Atomically dispersed metal catalysts for the oxygen reduction reaction: synthesis, characterization, reaction mechanisms and electrochemical energy applications. *Energy & Environmental Science*, 12(10): 2890–2923
- Liu W, Gong Y, Tricker A, Wu G, Liu C, Chao Z, Deng Y (2020). Fundamental study toward improving the performance of a high-moisture biomass-fueled redox flow fuel cell. *Industrial & Engineering Chemistry Research*, 59(10): 4817–4828
- Liu W, Mu W, Deng Y (2014a). High-performance liquid-catalyst fuel cell for direct biomass-into-electricity conversion. *Angewandte Chemie (International ed. in English)*, 53(49): 13558–13562
- Liu W, Mu W, Liu M, Zhang X, Cai H, Deng Y (2014b). Solar-induced direct biomass-to-electricity hybrid fuel cell using polyoxometalates as photocatalyst and charge carrier. *Nature Communications*, 5(1): 3208
- Lu L, Guest J S, Peters C A, Zhu X P, Rau G H, Ren Z Y (2018). Wastewater treatment for carbon capture and utilization. *Nature Sustainability*, 1(12): 750–758
- Mohamed M, Salama T, Hegazy M, Abou Shahba R, Mohamed S (2019). Synthesis of hexagonal WO₃ nanocrystals with various morphologies and their enhanced electrocatalytic activities toward hydrogen evolution. *International Journal of Hydrogen Energy*, 44(10): 4724–4736
- Munoz-Cupa C, Hu Y, Xu C, Bassi A (2021). An overview of microbial fuel cell usage in wastewater treatment, resource recovery and energy production. *Science of the Total Environment*, 754: 142429–142450
- Naseri N, Yousefzadeh S, Daryaei E, Moshfegh A Z (2011). Photo response and H₂ production of topographically controlled PEG assisted Sol-gel WO₃ nanocrystalline thin films. *International Journal of Hydrogen Energy*, 36(21): 13461–13472
- Parmar J, Jang S, Soler L, Kim D P, Sánchez S (2015). Nanophotocatalysts in microfluidics, energy conversion and environmental applications. *Lab on a Chip*, 15(11): 2352–2356
- Rengifo-Herrera J A, Blanco M, Wist J, Florian P, Pizzio L R (2016). TiO₂ modified with polyoxotungstates should induce visible-light absorption and high photocatalytic activity through the formation of surface complexes. *Applied Catalysis B: Environmental*, 189: 99–109
- Sadakane M, Steckhan E (1998). Electrochemical properties of polyoxometalates as electrocatalysts. *Chemical Reviews*, 98(1):

- 219–238
- Shen Z, Li F, Lu J, Wang Z, Li R, Zhang X, Zhang C, Wang Y, Wang Y, Lv Z, Liu J, Fan C (2021). Enhanced N₂ photofixation activity of flower-like BiOCl by in situ Fe(III) doped as an activation center. *Journal of Colloid and Interface Science*, 584: 174–181
- Song I K, Barteau M A (2004). Redox properties of Keggin-type heteropolyacid (HPA) catalysts: effect of counter-cation, heteroatom, and polyatom substitution. *Journal of Molecular Catalysis A, Chemical*, 212(1–2): 229–236
- Symes M D, Cronin L (2013). Decoupling hydrogen and oxygen evolution during electrolytic water splitting using an electron-coupled-proton buffer. *Nature Chemistry*, 5(5): 403–409
- Vadivel S, Naveen A N, Theerthagiri J, Madhavan J, Santhoshini Priya T, Balasubramanian N (2016). Solvothermal synthesis of BiPO₄ nanorods/MWCNT (1D-1D) composite for photocatalyst and supercapacitor applications. *Ceramics International*, 42(12): 14196–14205
- Wang H, Xie W, Yu B, Qi B, Liu R, Zhuang X, Liu S, Liu P, Duan J, Zhou J (2021). Simultaneous solar steam and electricity generation from synergistic salinity-temperature gradient. *Advanced Energy Materials*, 11(18): 2100481–2100487
- Wang Q, Wang W, Zhong L L, Liu D M, Cao X Z, Cui F Y (2018). Oxygen vacancy-rich 2D/2D BiOCl-g-C₃N₄ ultrathin heterostructure nanosheets for enhanced visible-light-driven photocatalytic activity in environmental remediation. *Applied Catalysis B, Environmental*, 220: 290–302
- Wang Y, Pang Y, Xu H, Martinez A, Chen K (2022). PEM Fuel cell and electrolysis cell technologies and hydrogen infrastructure development: a review. *Energy & Environmental Science*, 15(6): 2288–2328
- Xu Y, Xu S, Wang S, Zhang Y, Li G (2014). Citric acid modulated electrochemical synthesis and photocatalytic behavior of BiOCl nanoplates with exposed 001 facets. *Dalton Transactions (Cambridge, England)*, 43(2): 479–485
- Yang W, Du X, Liu W, Tricker A, Dai H, Deng Y (2019a). High efficient lignin depolymerization via effective inhibition of condensation during polyoxometalate mediated oxidation. *Energy & Fuels*, 33(7): 6483–6490
- Yang W, Du X, Liu W, Wang Z, Dai H, Deng Y L (2019b). Direct valorization of lignocellulosic biomass into value-added chemicals by polyoxometalate catalyzed oxidation under mild conditions. *Industrial & Engineering Chemistry Research*, 58(51): 22996–23004
- Zeng Q, Chang S, Beyhaqi A, Wang M, Hu C (2020). Efficient electricity production coupled with water treatment via a highly adaptable, successive water-energy synergistic system. *Nano Energy*, 67: 104237–104247
- Zhang L, Wong K, Chen Z, Yu J, Zhao J, Hu C, Chan C, Wong P (2009). AgBr-Ag-Bi₂WO₆ nanojunction system: A novel and efficient photocatalyst with double visible-light active components. *Applied Catalysis A, General*, 363(1–2): 221–229
- Zhang X Y, Guo X G, Wang Q Y, Zhang R F, Xu T, Liang P, Huang X (2020). Iron-based clusters embedded in nitrogen doped activated carbon catalysts with superior cathodic activity in microbial fuel cells. *Journal of Materials Chemistry A, Materials for Energy and Sustainability*, 8(21): 10772–10778
- Zhang X, Xia X, He W, Huang X, Logan B E (2017). Addition of conductive particles to improve the performance of activated carbon air-cathodes in microbial fuel cells. *Environmental Science. Water Research & Technology*, 3(5): 806–810
- Zheng Q, Durkin D P, Elenewski J E, Sun Y, Banek N A, Hua L, Chen H, Wagner M J, Zhang W, Shuai D (2016). Visible-light-responsive graphitic carbon nitride: rational design and photocatalytic applications for water treatment. *Environmental Science & Technology*, 50(23): 12938–12948
- Zhou C Y, Lai C, Xu P, Zeng G M, Huang D L, Zhang C, Cheng M, Hu L, Wan J, Liu Y, Xiong W P, Deng Y C, Wen M (2018a). In Situ Grown AgI/Bi₁₂O₁₇Cl₂ heterojunction photocatalysts for visible light degradation of sulfamethazine: efficiency, pathway, and mechanism. *ACS Sustainable Chemistry & Engineering*, 6(3): 4174–4184
- Zhou Y, Ji Q, Liu H, Qu J (2018b). Pore structure-dependent mass transport in flow-through electrodes for water remediation. *Environmental Science & Technology*, 52(13): 7477–7485
- Zhou Y, Zhang G, Ji Q, Zhang W, Zhang J, Liu H, Qu J (2019). Enhanced stabilization and effective utilization of atomic hydrogen on Pd-In nanoparticles in a flow-through electrode. *Environmental Science & Technology*, 53(19): 11383–11390
- Zu X H, Sun L L, Gong J, Liu X C, Liu Y X, Du X, Liu W, Chen L F, Yi G B, Zhang W G, et al. (2018). Ferric ion pair mediated biomass redox flow fuel cell and related chemical reaction kinetics study. *Chemical Engineering Journal*, 348: 476–484